Chinese Chemical Letters 35 (2024) 109681

Contents lists available at ScienceDirect

Chinese Chemical Letters

journal homepage: www.elsevier.com/locate/cclet

Self-calibrating probes constructed on a unique dual-emissive fluorescence platform for the precise tracking of cellular senescence

Xu Qu[a,1], Pengzhao Wu[a,1], Kaixuan Duan[a,1], Guangwei Wang[a], Liang-Liang Gao[a], Yuan Guo[a,*], Jianjian Zhang[a,*], Donglei Shi[a,b,*]

[a] Key Laboratory of Synthetic and Natural Functional Molecule of the Ministry of Education, College of Chemistry and Materials Science, Northwest University, Xi'an 710127, China
[b] Key Laboratory of Tropical Biological Resources of Ministry of Education, School of Pharmaceutical Sciences, Hainan University, Haikou 570228, China

ARTICLE INFO

Article history:
Received 20 December 2023
Revised 19 February 2024
Accepted 21 February 2024
Available online 5 March 2024

Keywords:
Senescence associated β-galactosidase
Dual-emission
Self-calibration
Cell imaging
Fluorescent probes

ABSTRACT

Human β-galactosidase (β-gal) is recognized as a crucial biomarker for evaluating senescence at the cellular and tissue levels in humans. However, tools to precisely track the endogenous β-gal are still limited. Herein, we present two novel self-calibrating β-gal probes **7a** and **7b** which were constructed on a unique green/red dual-emissive fluorescence platform. The two probes inherently exhibited a stable green fluorescence signal impervious to β-gal activity, serving as a reliable internal reference. They also displayed a progressively diminishing red fluorescence signal with the increasing of β-gal expression levels. The dual behavior endows them with self-calibration capacity and then renders excellently selective and sensitive for precisely monitoring β-gal activity. Notably, compared with *E. coli* β-gal, the two probes are more effectively response to *A. oryzae* β-gal homologous to human β-gal, indicating their unique species-selectivity. Furthermore, **7a** was validated for its effectiveness in determining senescence-associated β-galactosidase (SA-β-gal) expression in senescent NRK-52E and HepG2 cells, underscoring its practical applicability in senescence research.

© 2024 Published by Elsevier B.V. on behalf of Chinese Chemical Society and Institute of Materia Medica, Chinese Academy of Medical Sciences.

Cellular senescence is a distinct state induced by stress and various physiological processes. It is hallmarked by irreversible cell-cycle arrest, unique secretion characteristics, macromolecular damage and metabolic alterations [1–3]. Senescent cells (SnCs) play a critical role in embryonic development, tissue repair and cancer prevention. However, the excessive accumulation of SnCs contributes to aging, dysfunction, and the onset of aging-related diseases [4]. Despite being metabolically and transcriptionally active, SnCs undergo significant morphological and gene expression changes, adopting a distinctive secretory phenotype [5,6]. The expression of specific proteins, including p16 [7], p21 [8], interleukin 6 (IL-6) [9], histone variant macroH2A (macroH2A) [10], phosphorylated γ-histone 2AX (γ-H2AX) [11], phosphorylated p38 mitogen activated protein kinase (p38 MAPK) [12] and senescence-associated β-galactosidase (SA-β-gal) [13], progressively increases during cellular senescence. Notably, human SA-β-gal, a glycoside hydrolase enzyme encoded by the *GLB1* gene and expressed in lysosomes [14,15], is recognized as a reliable biomarker and a key indicator for the visual tracking of cellular and tissue senescence in humans [16].

Among the current detection methods for β-galactosidase (β-gal), fluorescent probes are garnering significant interests for their excellent selectivity, high sensitivity, and superior spatial and temporal resolution [17–23]. There has been notable progress in the development of small-molecule fluorescent probes, which have been effectively utilized for imaging β-gal in living cells, organisms, and mice (Table S1 in Supporting information). However, many of these probes that respond to β-gal depended on the intensity variation at a single emission wavelength [24,25]. This reliance could lead to inaccuracies due to various factors such as light intensity fluctuation, fluorophore bleaching, and background interference [26]. In contrast, dual-emission fluorescent probes offer a more precise detection method, which circumvent these issues by self-calibration of dual-channel fluorescence intensity ratio [27]. However, self-calibrating probes capable to accurately monitor SA-β-gal activity in living cells by dual-emission are limited.

In this study, we developed two novel dual-emissive β-gal fluorescent probes **7a** and **7b** with self-calibration capability, in which benzo[*a*]xanthene was meticulously selected as the fluorescence skeleton [28] and the C–O glycosidic bond in β configuration was introduced as the recognition site. Of note, probes in the zwitte-

* Corresponding authors.
E-mail addresses: guoyuan@nwu.edu.cn (Y. Guo), zhangjj@nwu.edu.cn (J. Zhang), dongleishi@hainanu.edu.cn (D. Shi).
[1] These authors contributed equally to this work.

https://doi.org/10.1016/j.cclet.2024.109681
1001-8417/© 2024 Published by Elsevier B.V. on behalf of Chinese Chemical Society and Institute of Materia Medica, Chinese Academy of Medical Sciences.

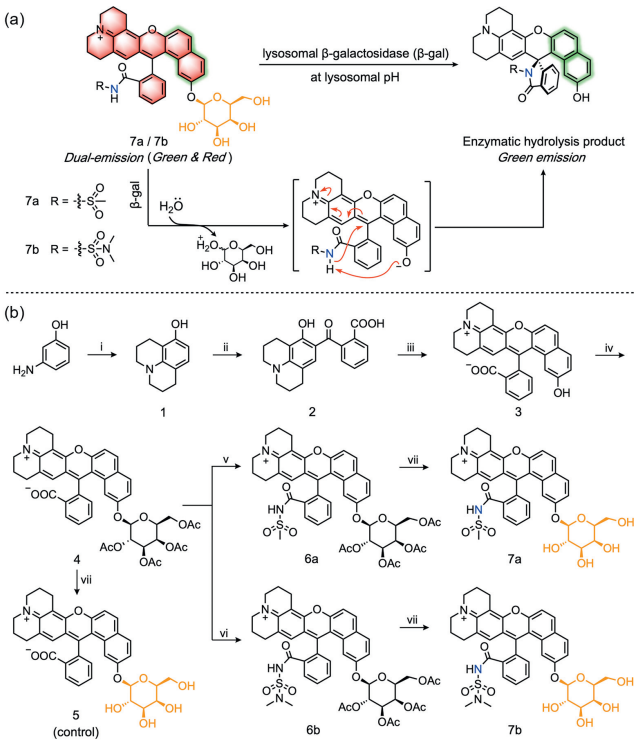

Fig. 1. (a) The proposed sensing mechanism of probes **7a** and **7b** toward lysosomal β-gal at lysosomal pH. (b) Synthesis routes of probes **7a**, **7b** and the control compound **5**. Reagents and conditions: (i) 1–chloro-3-bromopropane, *N*,*N*-dimethylformamide (DMF), Na_2CO_3, 70 °C; (ii) *o*-phthalic anhydride, toluene, reflux; (iii) 2,7-dihydroxyanphthalene, sulfuric acid, 90 °C; (iv) Cs_2CO_3, Na_2SO_4, CH_3CN, 2,3,4,6-tetra-*O*-acetyl-α-D-galactop-yranosyl-1-bromide, room temperature; (v) $POCl_3$, methylsulfamide, dry dichloromethane (DCM), dry CH_3CN, *N*,*N*-diisopropylethylamine (DIPEA); (vi) $POCl_3$, *N*,*N*-dimethylsulfamide, dry DCM, dry CH_3CN, DIPEA; (vii) K_2CO_3, MeOH, room temperature.

rionic form exhibited both green and red fluorescence emission. The green fluorescence should be emitted from the naphthol moiety which remained impervious to β-gal activity, ensuring that the green fluorescence intensity stayed essentially unchanged. This stable green signal served as a reliable internal reference throughout the detection process. Meanwhile, the β-gal-specific hydrolysis of the β-glycosidic bond pushed the probe into a spirocyclic-locked state, resulting in the red fluorescence intensity varying while the green fluorescence intensity unchanging with SA-β-gal changes. Consequently, the green fluorescence intensity was directly correlated with the concentrations of the probe, while the green/red fluorescence intensity ratios demonstrated a proportional relationship with the concentrations of the enzyme. Utilizing the green fluorescence signals enabled the precise determination of the concentration and distribution of the probe. Additionally, through a comparison of the dual-channel fluorescence ratio, a more accurate measurement of the enzyme content was achieved (Fig. 1a).

The synthesis of probes is meticulously illustrated in Fig. 1b. Initially, compounds **1** and **2** were synthesized as per methodologies outlined in our previous work [29]. Following this, compound **3** was obtained by the reaction of compound **2** with 2,7-dihydroxyanphthalene. Subsequently, compound **4** was generated *via* a nucleophilic substitution reaction involving compound **3** and 2,3,4,6-tetra-*O*-acetyl-α-D-galactopyranosyl bromide. To finely adjust the dynamic equilibrium of benzo[*a*]xanthene-based fluorescence scaffold, various electron-withdrawing groups (EWGs) were introduced, including methylsulfanilamide group and *N*,*N*-dimethylsulfanilamide group [30,31]. Thus, the next step involved the reaction of compound **4** with methylsulfamide and *N*,*N*-dimethylsulfamide, yielding compounds **6a** and **6b**, respectively. Finally, probes **7a** and **7b** and the control compound **5** containing a minor structural difference with probes (exposed carboxyl group) were gained *via* the deacetylation of compounds **6a**, **6b** and **4** in that order. By comparing the properties of **7a**, **7b** and **5**, we aimed to identify the optimal EWG to the construction of a desirable fluorescent probe. All synthesized compounds were rigorously characterized using ^{1}H NMR, ^{13}C NMR and high resolution mass spectrometry (HRMS) techniques (Figs. S13–S39 in Supporting information).

We initially explored the influence of pH on the optical properties of probes and the control. The control compound **5** consistently exhibited strong red fluorescence across a wide physiological pH range of 2–11, peaking at 617 nm (Fig. S1 in Supporting information). Conversely, probes **7a** and **7b** displayed both strong red fluorescence (at 611 nm for **7a** and 605 nm for **7b**) and green fluorescence (at 523 nm for **7a** and 521 nm for **7b**) in phosphate-buffer saline (PBS) across various pH values. The fluorescence intensity ratio of **7a** ($I_{523\ nm}/I_{611\ nm}$) remained constant over the physiological pH range of 4–9, while that of **7b** ($I_{521\ nm}/I_{605\ nm}$) showed irregular fluctuations within this range (Figs. S2 and S3 in Supporting information). The findings indicated that probe **7a** maintains stable fluorescence properties, predominantly emitting red fluorescence compared with **7b**.

Subsequent investigations into the absorption and emission spectra of these compounds were investigated in PBS buffer (100 mmol/L, pH 4.5) at 37 °C before and after the addition of *A. oryzae* β-gal, respectively. All compounds showed maximum absorption at the range of 400–600 nm and displayed remarkable change in intensity upon the addition of *A. oryzae* β-gal (Fig. S4 in Supporting information). They emitted red fluorescence at 611 nm (for **7a**), 605 nm (for **7b**) and 617 nm (for **5**) and green fluorescence at 523 nm (for **7a**), 521 nm (for **7b**) and 524 nm (for **5**), respectively. The fluorescence of red channel was quenched gradually with the increase of the concentration of *A. oryzae* β-gal (0–50 U), while the green fluorescence remained relatively constant. The fluorescence intensity ratio of both probes ($I_{523\ nm}/I_{611\ nm}$ for **7a** and $I_{521\ nm}/I_{605\ nm}$ for **7b**) significantly increased. Furthermore, a good linear relationship ($R^2 > 0.98$) was observed between the fluorescence intensity ratio and the concentration of *A. oryzae* β-gal (0–50 U), as depicted in Fig. 2 and Fig. S5 (Supporting information). In contrast, no such linear relationship was found for compound **5**. These results demonstrate the effective response of probes **7a** and **7b** to *A. oryzae* β-gal.

In addition, we evaluated the response of **7a**, **7b** and compound **5** to *E. coli* β-gal, a bacteria enzyme encoded by *lacZ* gene. As illustrated in Fig. S6 (Supporting information), the addition of *E. coli* β-gal resulted in a stable green fluorescence for both **7a** and **7b**, while their red fluorescence intensity progressively decreased. In contrast, compound **5** did not exhibit any significant signal changes under similar conditions. This observed linear response indicates that **7a** and **7b** are more effectively response to *A. oryzae* β-gal homologous to human β-gal compared to *E. coli* β-gal [14], suggesting that our probes exhibit unique species selectivity.

Given that the domain structure of *A. oryzae* β-gal instead of *E. coli* β-gal is akin to that of human β-gal and has the same optimal pH to human β-gal [14,32], We selected *A. oryzae* β-gal as the enzyme model in the following *in-vitro* assays. The reaction kinetics of **7a** and **7b** to *A. oryzae* β-gal were then analyzed. As shown in Figs. 3a and b and Fig. S7 (Supporting information), upon the addition of *A. oryzae* β-gal, the fluorescence intensity ratio of both probes showed a remarkable enhancement and reached a platform within 15 min for **7a** and within 6 min for **7b**. Similarly, the red channel fluorescence intensity of both probes progressively decreased and reached a steady state within the same frames, indicating their rapid response ability to *A. oryzae* β-gal.

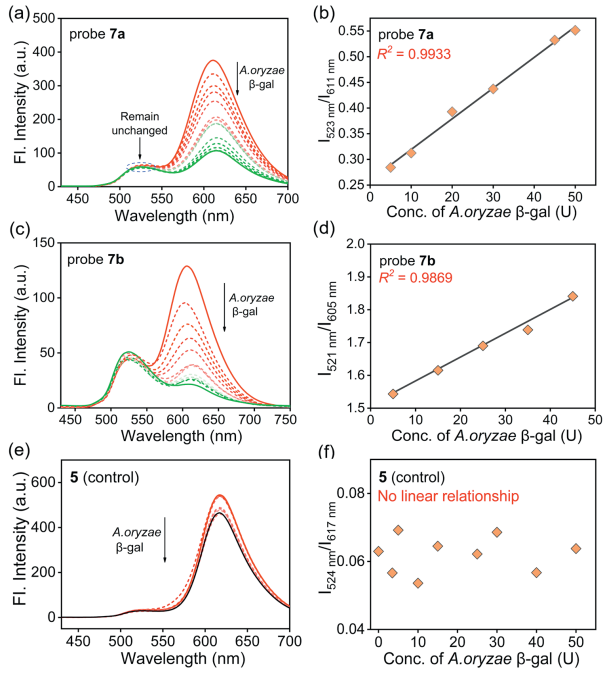

Fig. 2. (a) Fluorescence spectra of the probe **7a** (10 μmol/L) upon addition of *A. oryzae* β-gal (0–50 U), λ_{ex} = 408 nm. (b) The linear relationship between the fluorescence intensity ratio ($I_{523\ nm}/I_{611\ nm}$) and the concentration of *A. oryzae* β-gal. (c) Fluorescence spectra of the probe **7b** (10 μmol/L) upon addition of *A. oryzae* β-gal (0–45 U), λ_{ex} = 408 nm. (d) The linear relationship between the fluorescence intensity ratio ($I_{521\ nm}/I_{605\ nm}$) and the concentration of *A. oryzae* β-gal. (e) Fluorescence spectra of compound **5** (10 μmol/L) upon addition of *A. oryzae* β-gal (0–50 U), λ_{ex} = 408 nm. (f) the linear relationship between the fluorescence intensity ratio ($I_{524\ nm}/I_{617\ nm}$) and the concentration of *A. oryzae* β-gal. Slit: 5 nm/10 nm.

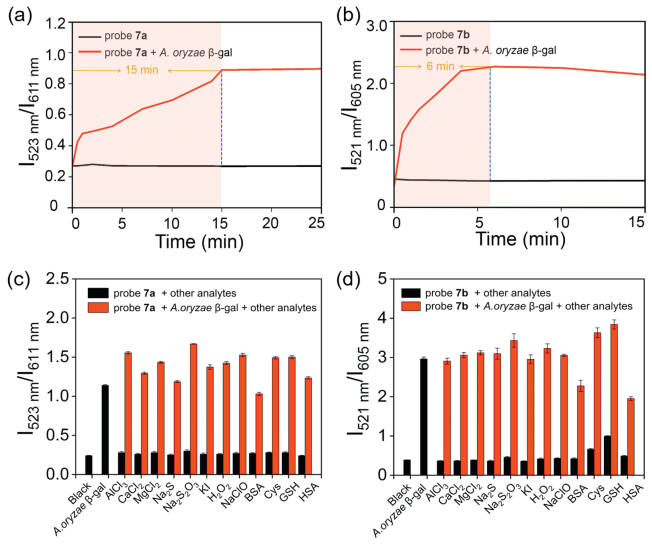

Fig. 3. (a) Time course of the fluorescence intensity ratio ($I_{523\ nm}/I_{611\ nm}$) of the probe **7a** (10 μmol/L) to *A. oryzae* β-gal (50 U) in PBS buffer (100 mmol/L, pH 4.5). λ_{ex} = 408 nm. (b) Time course of the fluorescence intensity ratio ($I_{521\ nm}/I_{605\ nm}$) of the probe **7b** (10 μmol/L) to *A. oryzae* β-gal (50 U) in PBS buffer (100 mmol, pH 4.5). λ_{ex} = 408 nm; slit: 5 nm/10 nm. (c) Corresponding fluorescence intensity ratio ($I_{523\ nm}/I_{611\ nm}$) of the probe **7a** (10 μmol/L) to different species. λ_{ex} = 408 nm; slit: 5 nm/10 nm. (d) Corresponding fluorescence intensity ratio ($I_{521\ nm}/I_{605\ nm}$) of the probe **7b** (10 μmol/L) to different species. λ_{ex} = 408 nm; slit: 5 nm/10 nm. The different species including *A. oryzae* β-gal, $AlCl_3$, $CaCl_2$, $MgCl_2$, Na_2S, $Na_2S_2O_3$, KI, H_2O_2, NaClO, bovine serum albumin (BSA), cysteine (Cys), glutathione (GSH) and human serum albumin (HSA, purchased from Nanjing Duly Biotech Co., Ltd.).

Next, we carried out selectivity and competition studies for **7a** and **7b**. When various potential interfering analytes were introduced, the fluorescence intensity ratio of both probes ($I_{523\ nm}/I_{611\ nm}$ for **7a** and $I_{521\ nm}/I_{605\ nm}$ for **7b**) displayed negligible changes. However, remarkable changes were observed in the presence of *A. oryzae* β-gal. Moreover, the spectral profiles of both probes remained unaffected when co-incubated with *A. oryzae* β-gal and other analytes, underscoring their high selectivity for the target enzyme (Figs. 3c and d, Fig. S8 in Supporting information). These results conclusively demonstrated that **7a** and **7b** possess high selectivity for *A. oryzae* β-gal and hold promise for the precise detection of human β-gal in complex biological systems.

HRMS titration analysis was subsequently conducted to validate the proposed sensing mechanism. Upon the addition of *A. oryzae* β-gal to **7a**, the original signal peak at *m/z* 723.1976 corresponding to the [**7a**+Na]$^+$ vanished, and a new signal peak appeared at *m/z* 561.1473, attributable to the enzymatic hydrolysis product. A similar outcome was obtained for **7b**, confirming that both probes can be hydrolyzed by *A. oryzae* β-gal (Fig. S9 in Supporting information).

In comparing the optical properties of both probes, probe **7a** demonstrated superior characteristics over **7b**. Hence, **7a** was selected for the subsequent live-cell imaging experiments. Prior to cellular imaging, the cytotoxicity of **7a** towards NRK-52E cells and HepG2 cells were evaluated and the results showed their negligible cytotoxic effects and excellent biocompatibility (Fig. S10 in Supporting information). To obtain the senescent cell model, NRK-52E cells were treated with mitomycin C (Mito C) [33], a widely used DNA-damage inducer. The overexpression of SA-β-gal in these senescent cells was confirmed using the X-gal staining assay. Then, young and Mito C-treated NRK-52E cells were stained with **7a**. As depicted in Fig. 4, the average fluorescence intensity of senescent cells was indeed much higher than that of young cells in the green or red channel, while the reproducibility was poor and the errors are large. To our delight, the fluorescence intensity ratio (I_{Green}/I_{Red}) of the senescent NRK-52E cells was about 1.3-fold higher than that of the young NRK-52E cells and had a nice reproducibility, achieving more reliable detection result. In addition, phenylethyl β-D-thiogalactopyranoside (PETG) and D-galactose as competitive inhibitors [34] were employed to suppress β-gal activity in senescent cells respectively, resulting in lower fluorescence intensity and fluorescence ratio compared to Mito C-induced senescent cells. Additionally, similar experiments with **7a** were conducted on HepG2 cells, which were induced into senescence using XL413, a DNA-replication kinase CDC7 inhibitor [35]. The results mirrored those observed in NRK-52E cells, as seen in Fig. S11 (Supporting information), suggesting the potential of **7a** as a robust tool for monitoring SA-β-gal during cellular senescence.

Furthermore, the subcellular localization capacity of **7a** was investigated in both senescent NRK-52E and HepG2 cells through co-staining with commercial LysoTracker Deep Red and MitoTracker Deep Red. The imaging results revealed a high degree of overlap between the red channel fluorescence of **7a** and the fluorescence of LysoTracker in the near-infrared (NIR) channel, with high Pearson's correlation coefficient (PCC) values of 0.88 in senescent NRK-52E cells and 0.89 in senescent HepG2 cells. In contrast, the red channel fluorescence partially overlapped with the fluorescence of MitoTracker Deep Red, showing lower PCC values of 0.48 in senescent NRK-52E cells and 0.42 in senescent HepG2 cells. These findings confirmed the excellent lysosome-targeting ability of **7a** as a lysosomal enzyme (SA-β-gal) probe (Fig. 4 and Fig. S12 in Supporting information).

In summary, we have successfully developed two SA-β-gal fluorescent probes **7a** and **7b**, characterized by their green/red dual-emission. The two probes are innovatively designed by incorporating benzo[*a*]xanthene modified with sulfonamide as the fluo-

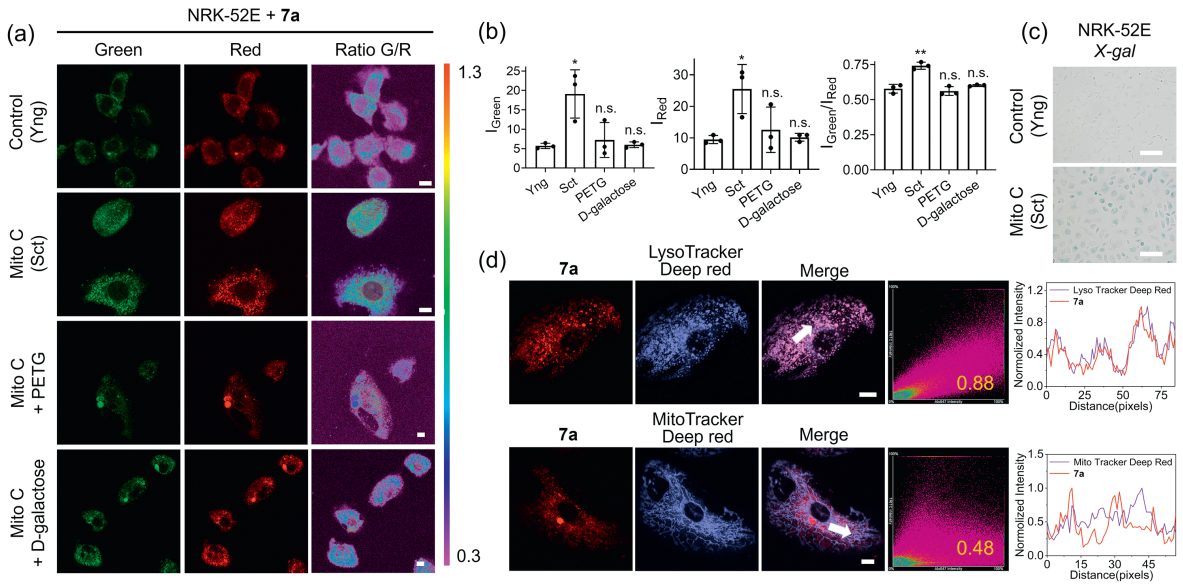

Fig. 4. (a) Rows 1 and 2: confocal fluorescence images of young (Yng) NRK-52E cells and Mito C-induced senescent (Sct) NRK-52E cells after incubation with **7a** (7.5 μmol/L) for 20 min. Rows 3 and 4: confocal fluorescence images of Mito C-induced senescent (Sct) NRK-52E cells treated with PETG (1 mmol/L) or D-galactose (1 μmol/L) for 2 h and then incubated with **7a** (7.5 μmol/L) for 20 min. Scale bar: 10 μm. (b) Quantification of the fluorescence intensity in the green/red channel and fluorescence intensity ratio (I_{Green}/I_{Red}) in each group. Error bars represent the standard deviation (± S.D.) with $n = 3$. Significant differences (n.s., not significant. $^{*}P < 0.05$, $^{**}P < 0.01$ *vs.* Yng) are analyzed with two-sided Student's *t*-test. (c) X-gal staining images of young NRK-52E cells and Mito C-induced senescent NRK-52E cells. Scale bar: 100 μm. (d) Colocalization studies of senescent NRK-52E cells co-stained with LysoTracker Deep Red (75 nmol/L, 30 min)/MitoTracker Deep Red (100 nmol/L, 30 min) and **7a** (7.5 μmol/L, 20 min) on a Nikon A1 laser-scanning confocal microscope. Scale bar: 10 μm. Green channel: $\lambda_{ex} = 408$ nm, $\lambda_{em} = 500–550$ nm. Red channel: $\lambda_{ex} = 488$ nm, $\lambda_{em} = 570–620$ nm. NIR channel: $\lambda_{ex} = 640$ nm, $\lambda_{em} = 663–738$ nm.

rescence reporter and a β-gal cleavable unit as the enzyme-active trigger. A key advantage of both probes is their dual-emission feature, enabling the precise detection of SA-β-gal through the self-calibration. They exhibited a stable green emission serving as an internal reference and meanwhile showed a progressively decreasing red fluorescence signal in response to β-gal with an excellent linear relationship ($R^2 > 0.98$). Better still, **7a** was successfully employed for the fluorescence imaging of SA-β-gal in senescent NRK-52E and HepG2 cells. This study offers a novel strategy and method for designing SA-β-gal fluorescent probes with superior sensing performance and optical properties. The development of such probes featuring self-calibration capabilities holds promise for significant advancements in diagnostic and therapeutic applications.

Declaration of competing interest

The authors declare that they have no known competing financial interests or personal relationships that could have appeared to influence the work reported in this paper.

Acknowledgments

We gratefully appreciate the financial support from the National Natural Science Foundation of China (Nos. 21977082, 22037002 and 21472148), the Natural Science Basic Research Program of Shaanxi (No. 2020JC-38).

Supplementary materials

Supplementary material associated with this article can be found, in the online version, at doi:10.1016/j.cclet.2024.109681.

References

[1] Z.H. Li, J. Cheng, P. Huang, et al., Chin. Chem. Lett. 34 (2023) 109153.
[2] H.T. Kang, J.T. Park, K. Choi, et al., Nat. Chem. Biol. 13 (2017) 616–623.
[3] Y.T. Wang, H.M. Yan, Y.K. Yue, et al., Chem. Eng. J. 464 (2023) 142496.
[4] J. Meng, Z.Y. Lv, X.H. Qiao, et al., Redox Biol. 11 (2017) 365–374.
[5] A.V. Borodkina, A.N. Shatrova, P.I. Deryabin, et al., Aging 12 (2016) 3400–3418.
[6] J.C. Wang, J. Wei, H. Inuzuka, Acta Mater. Med. 3 (2023) 281–284.
[7] D. Kusumoto, T. Seki, H. Sawada, et al., Nat. Commun. 12 (2021) 257.
[8] M. Althubiti, L. Lezina, S. Carrera, et al., Cell Death Dis. 5 (2014) e1528.
[9] J.K. Kiecolt-Glaser, K.J. Preacher, R.C. MacCallum, et al., Proc. Natl. Acad. Sci. U. S. A. 100 (2003) 9090–9095.
[10] R.G. Zhang, M.V. Poustovoitov, X.F. Ye, et al., Dev. Cell 8 (2005) 19–30.
[11] U. Herbig, M. Ferreira, L. Condel, D. Carey, J.M. Sedivy, Science 311 (2006) 1257.
[12] Y. Suh, Mech. Ageing Dev. 122 (2001) 1797–1811.
[13] Y. Gao, Y.L. Hu, Q.M. Liu, et al., Angew. Chem. Int. Ed. 60 (2021) 10756–10765.
[14] X.K. Li, W.J. Qiu, J.W. Li, et al., Chem. Sci. 11 (2020) 7292–7301.
[15] H.T. Pang, X.Z. Chai, J.J. Zhang, Chin. Chem. Lett. 34 (2023) 108321.
[16] D.L. Shi, W.W. Liu, G.W. Wang, Y. Guo, J. Li, Acta Mater. Med. 1 (2022) 4–23.
[17] X.Y. Zhao, M.B. Ding, L.L. Ning, et al., Acta Mater. Med. 4 (2022) 476–485.
[18] Y.C. Wu, C.X. Yin, W.J. Zhang, Y.B. Zhang, F.J. Huo, Anal. Chem. 94 (2022) 5069–5074.
[19] G.Y. Jiang, G.J. Zeng, W.P. Zhu, et al., Chem. Commun. 53 (2017) 4505–4508.
[20] L.T. Zeng, T.H. Chen, B.T. Zhu, et al., Chem. Sci. 13 (2022) 4523–4532.
[21] C. Duan, M. Won, P. Verwilst, et al., Anal. Chem. 91 (2019) 4172–4178.
[22] L.R. Jiang, T.H. Chen, E.W. Song, et al., Chem. Eng. J. 427 (2022) 131563.
[23] Y.Y. Sun, X.N. Zhou, L.Y. Sun, et al., Chin. Chem. Lett. 33 (2022) 4229–4232.
[24] Y. Li, L.L. Ning, F. Yuan, et al., Anal. Chem. 92 (2020) 5733–5740.
[25] J.J. Zhang, P.H. Cheng, K.Y. Pu, Bioconjugate Chem. 30 (2019) 2089–2101.
[26] X.Z. Chen, X.Y. Zhang, X.D. Ma, et al., Talanta 192 (2019) 308–313.
[27] K.Z. Gu, Y.S. Xu, H. Li, et al., J. Am. Chem. Soc. 138 (2016) 5334–5340.
[28] X.W. Li, H.M. Yan, F.J. Huo, et al., Analyst 148 (2023) 2465–2471.
[29] J.Y. Tian, D.L. Shi, Y.H. Zhang, et al., Chem. Sci. 12 (2021) 13483–13491.
[30] L. Wang, M. Tran, E. D'Este, et al., Nat. Chem. 12 (2020) 165–172.
[31] L. Wang, J. Hiblot, C. Popp, L. Xue, K. Johnsson, Angew. Chem. Int. Ed. 59 (2020) 21880–21884.
[32] J.D. Wang, F.J. Huo, Y.B. Zhang, C.X. Yin, Chin. Chem. Lett. 34 (2023) 107818.
[33] C. Wang, S. Vegna, H.J. Jin, et al., Nature 574 (2019) 268–272.
[34] D.L. Shi, W.W. Liu, Y. Gao, et al., Nat. Aging 3 (2023) 297–312.
[35] S.Y. Cheng, J. Seo, B.T. Huang, T. Napolitano, E. Champeil, Int. J. Oncol. 49 (2016) 1815–1824.